Development and validation of a microfluidic reactor for biofilm monitoring via optical methods



2011 J. Micromech. Microeng. 21 054023

(http://iopscience.iop.org/0960-1317/21/5/054023)

IOP Publishing Journal of Micromechanics and Microengineering

J. Micromech. Microeng. **21** (2011) 054023 (10pp) doi:10.1088/0960-1317/21/5/054023

# Development and validation of a microfluidic reactor for biofilm monitoring via optical methods

**Mariana T Meyer**[1,2], **Varnika Roy**[1,3], **William E Bentley**[1] and **Reza Ghodssi**[1,2,4]

[1] Fischell Department of Bioengineering, University of Maryland, College Park, MD 20742, USA
[2] Institute for Systems Research, University of Maryland, College Park, MD 20742, USA
[3] Graduate Program in Molecular and Cell Biology, University of Maryland, College Park, MD 20742, USA
[4] Department of Electrical and Computer Engineering, University of Maryland, College Park, MD 20742, USA

E-mail: ghodssi@umd.edu

Received 29 November 2010, in final form 2 April 2011
Published 28 April 2011
Online at stacks.iop.org/JMM/21/054023

**Abstract**

We present the design, fabrication, and verification of a microfluidic platform for optical monitoring of bacterial biofilms. Biofilm formation characterizes the majority of infections caused by bacteria that are developing increased resistance to traditional antibiotic treatment, necessitating the development of reliable tools not only for study of biofilm growth, but also for *in situ* examination of the response to applied stimuli. The presented platform was used to continuously and non-invasively observe the dependence of *Escherichia coli* biofilm formation on bacterial signaling by monitoring the change in biofilm optical density over the growth period. Results were corroborated by measurement of biofilm morphological properties via confocal microscopy, and statistical analysis was applied to verify the repeatability of observed optical and morphological differences in the biofilms formed. The presented platform will be used to characterize biofilm formation and response in drug discovery applications.

(Some figures in this article are in colour only in the electronic version)

## 1. Introduction

Many types of bacteria are able to communicate with each other through quorum sensing, a process involving the continuous secretion and uptake of signaling molecules. Through this communication, bacteria are able to determine the size of the surrounding population. Upon reaching a threshold population, the molecular signaling dictates a change in phenotype often resulting in the formation of a biofilm, a pathogenic matrix comprised mainly of extracellular polysaccharides and bacteria. Biofilms are of particular interest since they are clinically prevalent; it is estimated that biofilms are involved in 65% of bacterial infections in humans [1]. Clinically, biofilms are difficult to treat due to their increased resistance to traditional antibiotic treatment as compared to bacterial suspensions [2]. Since there exists a need for development of new, effective biofilm treatments, there also exists a need for *in vitro* biofilm models on which new pharmaceutical agents may be tested.

The majority of previously performed biofilm studies involve the use of macroscale reactors. Recently, there have been increased efforts to study bacterial biofilms in a microfluidic setting. Microfluidic systems provide several advantages, including inexpensive fabrication, highly parallel throughput, small size, and tight control over the microenvironment for cell culture [3]. Biofilms formed in microfluidics are commonly evaluated using sensitive but involved external instrumentation such as confocal microscopy [4–6], a technique also used to evaluate biofilms formed in macroscale biofilm models [7–9]. While microscopy provides relevant data as to the biofilm state, it often requires labeled samples. Additionally, without a permanent fixture on the

 

microscope, microscopy is an end-point measurement and cannot be performed continuously; instantaneous responses of the biofilm to stimuli are desirable in order to gain a more detailed understanding of the dynamics of biofilm response to new treatments under study.

Microfluidic systems are compatible with integration of microfabricated sensors, creating lab-on-a-chip platforms. These systems, by nature of being batch microfabricated, are small, inexpensive, and easily integrated with a multitude of sensing devices and methods. One of the most common types of sensors integrated in microfluidics is electrical biosensors, due to their ease of patterning and lack of moving parts that may malfunction during fluidic flow of biological samples. Electrical sensors have been implemented for monitoring cell sedimentation, adhesion, and growth [10–13]. As cells adhere to a surface, the spread of the cell reduces the dielectric layer thickness, increasing the capacitance. Electrical sensors may be arrayed and integrated on-chip with signal processing circuitry, allowing for a compact cell sensing device [10], may be integrated into microfluidics for evaluation of cell deposition and proliferation in a flow environment [11, 12], and functionalized to allow for sensor specificity [12, 13]. While the above sensors are very sensitive, interpretation of the data is not completely independent of the media used within the channel and additionally requires involved signal processing for evaluating the frequency-dependent response of the sensor.

While there are many possible ways to observe a bacterial biofilm, our group has pursued optical absorbance quantification of biofilms along with morphological properties via confocal imaging. Bakke *et al* formed biofilms in macroscale fluidic reactors and measured the optical density at selected time points [14]; optical thickness was measured and found to be correlated to the biofilm optical absorbance measured at 420 nm. The optical density changes observed were hypothesized to be due to the turbidity of the solution, in addition to light scattered by the uneven surface of the biofilm. While the work utilized discrete measurements of biofilm absorbance as opposed to continuous, real-time measurements, it demonstrates the viability of biofilm monitoring via optical absorbance. Additionally, this method is capable of being easily implemented using inexpensive optical components (i.e. a light source and a photodetector) and the biofilm growth is interpreted as an increase or decrease in photodetector output.

Studies performed on biofilm formation typically are conducted as demonstrations, since biofilm formation is considered highly irregular and non-reproducible. While some work has investigated the reproducibility of biofilm morphology in flow conditions [15] and the correlation between biofilm optical density and carbon content [8], to the best of the authors' knowledge there has been no investigation of morphology or optical density reproducibility in microfluidic biofilm reactors.

In this work, we present a platform that leverages the properties of microfluidics and combines them with the unique capability of measuring the optical density of biofilms formed in the microfluidic environment. Biofilm optical density is continuously and non-invasively measured using a simplified experimental setup using off-the-shelf electrical components. Biofilm optical properties are corroborated with biofilm morphological properties quantified using confocal microscopy and image analysis. The platform is used to investigate the dependence of *Escherichia coli* biofilm formation on quorum sensing, which is the process used to describe bacterial communication. This investigation is achieved by comparing optical and morphological data between wild-type *E. coli* and *E. coli* incapable of quorum sensing molecule synthesis. The quorum sensing molecule under investigation, AI-2 (autoinducer-2), is known to exert control over the signaling of more than 70 species of bacteria; thus, our results can be extended to relate to a wide variety of bacterial systems [16]. The repeatability of biofilms formed in the platform using the developed methodology is also evaluated, toward the end of using the system as a reliable drug evaluation platform.

## 2. Experimental details

### *2.1. Microfluidic platform design and fabrication*

The microfluidic platform, previously presented in [17], consists of a micropatterned base and a molded microfluidic channel. A coverslip serves as the base, providing a substrate that is both transparent and thin enough (150 $\mu$m) for using a confocal microscope to observe the biofilm at high resolution. 200 nm of chrome is sputtered onto the coverslip and patterned to provide two 200 $\mu$m $\times$ 200 $\mu$m windows using contact photolithography followed by chrome etching. The two patterned areas in each channel serve as observation windows, through which the optical density of the biofilm is measured. Patterned observation windows allow for repeatable positioning of measurements along the length of the microfluidic channel.

The microfluidic channel is constructed using molded polydimethylsiloxane (PDMS). The mold is fabricated by patterning 100 $\mu$m -thick SU8-50 on silicon using contact photolithography. PDMS (Sylgard 184, Dow Corning), in a 10:1 ratio of resin to curing agent, is poured onto the mold, cured at 80 °C for 20 min, then removed from the mold and cut to fit over the patterned coverslip. The resulting microfluidic channel is 100 $\mu$m deep, 500 $\mu$m wide, and 2 cm long. Ports for connecting the microfluidic channel to Tygon tubing are drilled into the PDMS using a 2 mm dermatological punch. The PDMS is reversibly bonded to the unpatterned side of the coverslip by applying methanol to the PDMS layer, then aligning and placing it onto the chip. Reversible bonding allows for disassembly, cleaning, and reuse of the patterned coverslip after it has been used for a biofilm formation experiment. A schematic of the microfluidic platform is shown in figure 1(*a*).

### *2.2. Platform assembly with external optical and fluidic elements*

Following fabrication, the platform is affixed to a glass slide, and the slide is aligned so that the observation windows in the coverslip are positioned over two external photodiodes (Digikey no 425-1937-ND). A transimpedance amplifier is

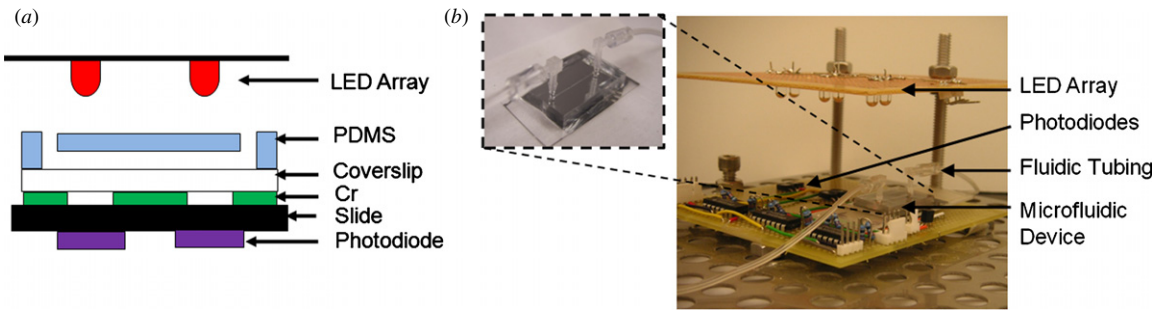


**Figure 1.** (*a*) Cross-sectional schematic of the microfluidic platform. The microfluidic channel molded in the PDMS layer is positioned on top of patterned measurement windows and aligned to external optical components. Layers are not drawn to scale. (*b*) Photograph of microfluidic device (inset) integrated with fluidic components, and positioned over photodiodes and under LEDs.

used to convert each photodiode current output to a voltage, which is connected to a data acquisition card (NI USB-6221). One end of Tygon tubing (Cole Parmer no 95609-14) is connected to barbed tubing connectors (Cole Parmer no 06365-15) and inserted into the port in the PDMS layer of the microfluidic device; the other end of one piece of tubing, designated the outlet, is connected to a syringe pump (Kent Scientific no KDS230) operating in withdrawal mode for minimizing leakage. The inlet tubing connects the microfluidic device to a reservoir of fluid held in a microcentrifuge tube. To aid in maintaining sterility and in transferring the tubing from one solution to the next, a steel capillary was inserted into the free end, used to pierce the top of the microcentrifuge tube, and sealed with paraffin film and epoxy.

An array of red LEDs is aligned to an array of microfluidic platforms; while biofilms have not been observed to possess characteristic absorbance peaks, the use of red LEDs (Digikey no 67-1612-ND), with peak emission at 660 nm and an intensity rating of 2800 mcd, is expected to minimize specific optical absorbance interactions with protein and DNA. The spacing between the tips of the LEDs and the top of the PDMS surface was approximately 2 cm during operating conditions. In the given system, the spacing was limited by the clearance needed for the fluidic tubing connectors. Provided the development of more compact packaging of both the fluidic connections and the LEDs and accompanying circuitry, this distance could ideally be decreased so that the light source is near flush with the surface of the PDMS, reducing scattering loss.

The entire assembly was placed inside an incubator at 37 °C. A photo of the platform setup is shown in figure 1(*b*).

### 2.3. Strains used

*E. coli* W3110 serves as the standard for biofilm formation. To probe the role of quorum sensing in optically detectable biofilm formation in microfluidics, a quorum sensing-null W3110 mutant, MDAI2 [18], is used. MDAI2 does not express *luxS*, one of the enzymes responsible for the synthesis of AI-2 (autoinducer-2), the primary quorum sensing signaling molecule used by *E. coli*. Restoration of quorum sensing capabilities is evaluated by adding 30 $\mu$M AI-2 to MDAI2 cultures; AI-2 was synthesized *in vitro* using LuxS and Pfs, both enzymes needed for complete synthesis of AI-2 [19]. During the operation of an experiment, the growth medium is refreshed every 12 h for all biofilms to ensure viability of the AI-2 molecules and to maintain parallelism between concurrent experiments. Bacterial cultures are grown to an $OD_{600}$ of 0.25. All cultures are grown in LB growth media.

### 2.4. Microfluidic platform operation

Prior to inoculation, the channel is disinfected by flowing 70% ethyl alcohol through the channel. The bacterial suspension, prepared as described above, is suctioned into the channel. The inoculum is incubated in the channel for 2 h with no flow to allow for bacterial adhesion to the substrate. The channel is rinsed with LB growth media for 15 min at a flow rate of 10 $\mu$L h$^{-1}$, corresponding to an average velocity of 0.06 mm s$^{-1}$ given the dimensions of the fabricated channel, to remove non-adherent cells. The platform is continuously operated at a flow rate of 10 $\mu$L h$^{-1}$ at 37 °C over the entire period of biofilm growth. Since the flow was created using a syringe pump in withdrawal mode (i.e. drawing fluid up from a reservoir, through the device, and into the syringe), refreshment of the media only required replacing a microcentrifuge tube of the growth media. To achieve this, flow was briefly stopped, and the fluidic tubing was carefully transferred from one tube to the other.

The initial optical absorbance of the biofilm is measured after the 15 min rinsing period, using the average of the photodiode output over a period of 15 min. The photodiode output is then continuously monitored and recorded using NI LabVIEW.

### 2.5. Microscopy and image analysis

At selected time points (12, 24, 36, 48, 60, and 72 h), biofilm growth is ceased. The channel is rinsed with deionized water at 10 $\mu$L h$^{-1}$. It is then treated with a Live/Dead Bacterial Labeling Kit (Invitrogen no L7012). The two fluorescent labeling components, SYTO9 and propidium iodide, are mixed in a 1:1 ratio to a final volume of 10 $\mu$L. The mixed components are introduced into the channel at 10 $\mu$L h$^{-1}$, and the dye is fixed by flowing 3% paraformaldehyde into the channel at the same flow rate. Labeled samples are imaged through each micropatterned window using a confocal microscope

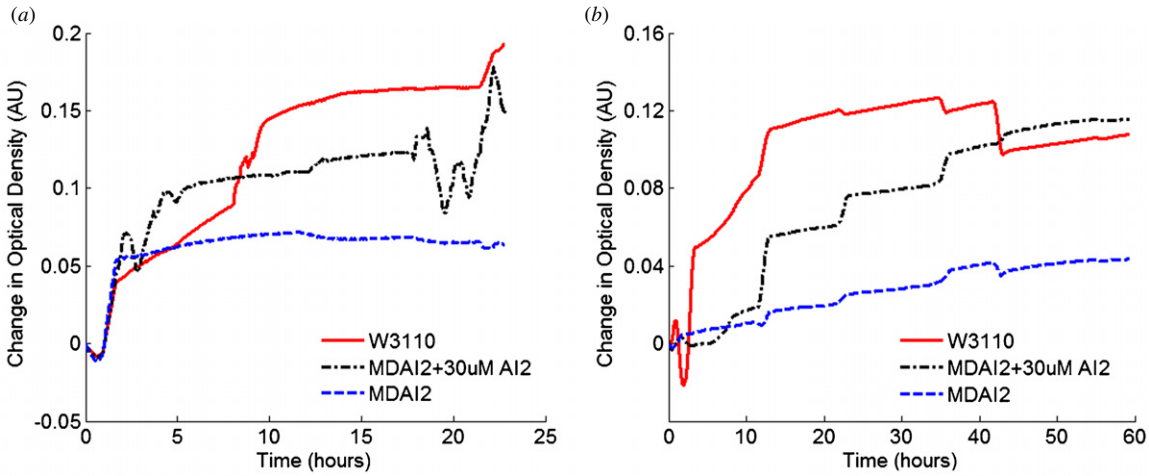


**Figure 2.** Raw optical density change measurements corresponding to two separate experiments, where W3110, MDAI2, and MDAI2 + AI2 biofilms were grown for (*a*) 24 h and (*b*) 60 h. End thicknesses of W3110, MDAI2, and MDAI2 + AI2 biofilms were approximately (*a*) 15, 14, 9.8 $\mu$m and (*b*) 30, 28, 8.5 $\mu$m, respectively.

(Zeiss LSM 710). Z-stacks are analyzed using COMSTAT to obtain the average thickness and roughness coefficient of the biofilm [20]. While COMSTAT is capable of calculating multiple properties of biofilms, thickness was selected as a characteristic measurement of biofilms that closely corresponds to the amount of biofilm present [4, 8, 14, 20]; the roughness coefficient, indicative of relative variation in the biofilm thickness, was also investigated as a potential metric for biofilm formation.

### *2.6. Data analysis*

Experiments were performed three times for each time point (12, 24, 36, 48, 60, and 72 h). Morphological and optical data are both reported as the average of values obtained at each of the two windows in a microfluidic channel. Net changes in optical density and thickness were compared between groups at each time point to evaluate significant differences. Since changes in optical density were continuously measured, 30 min averages centered around the time point of interest were used as data points for comparison. Changes from the baseline optical density and average thickness values were compared using Student's *t*-test. JMP® statistical analysis software was used for all statistical calculations.

## 3. Results and discussion

The presented method for evaluating bacterial biofilms based on optical density was used to observe several phenomena within a microfluidic flow cell.

### *3.1. Continuous monitoring of bacterial biofilm optical density*

The platform was used to investigate the role of quorum sensing in *E. coli* biofilm formation in microfluidics. Three platforms were arrayed in parallel; one was inoculated with wild-type *E. coli* W3110, and two with MDAI2. While the LB medium is flowed through all of the channels throughout growth, one of the channels inoculated with MDAI2 was exposed to the LB medium with 30 $\mu$M AI-2. The optical density of all three biofilms was continuously measured; samples of optical density data continuously obtained during these parallel experiments are shown in figure 2.

The platform developed and presented demonstrates the unique capability of continuously monitoring bacterial biofilms grown within microfluidics. This is exhibited by the sharp changes in recorded optical signals. Some of these sharp changes may be attributed to sloughing and redeposition of clumps of biofilm, such as those in figure 2(*a*) exhibited by MDAI2 biofilms grown with AI-2 between 17 and 24 h. Other sharp changes, such as the 'jags' seen approximately every 12 h in figure 2(*b*), may be attributed to the fact that growth media reservoirs were refreshed every 12 h for maintenance of AI-2 viability, and all reservoirs were replenished in order to maintain parallelism between experiments with and without AI-2 addition. The replenishment is thought to have a variable effect on bacterial growth in the microfluidic channel that may thereby alter the optical density over a short period of time.

Small differences were seen in the outputs of two photodiodes positioned at different locations within the microfluidic channel; an example of this is provided in figure 3(*a*). The windows are positioned 5 mm apart, with the first window 7.5 mm from the inlet. In this case, the output at the first window, closest to the inlet, shows more aberrations than the output of the second window. In other cases, such differences between photodiode outputs were not as apparent, as shown in figure 3(*b*), indicating that, at least in this work, firm conclusions with regard to repeatability in changes in biofilm properties along the length of the channel cannot be drawn.

In this study, the peak sensitivity of the photodiodes used was centered at 550 nm, while the peak emission of the LEDs was centered at 660 nm; while these components were chosen mainly for cost and availability reasons, it is expected that matching the peak wavelengths of the emitter and detector would increase the measurement sensitivity. The ideal experimental setup would include a photodiode with a

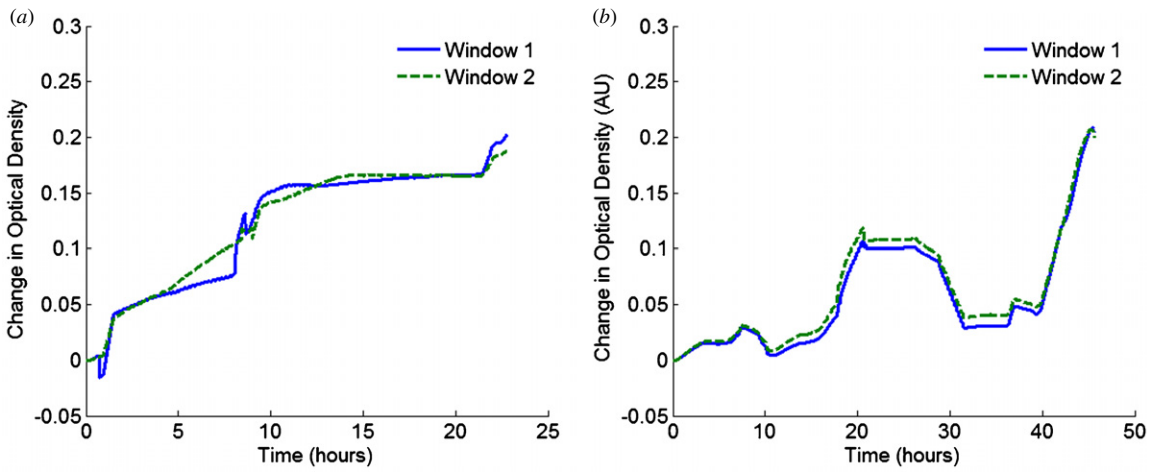


**Figure 3.** Raw optical density change measurements corresponding to the output of the two photodiodes positioned under one microfluidic channel. 'Window 1' is closest to the channel inlet. Data correspond to two separate *E. coli* W3110 experiments. (*a*) Outputs differ slightly along the length of the channel. (*b*) Outputs show almost identical behavior.

peak sensitivity at 660 nm, since there are fewer molecular absorption interactions in this range of the spectrum (e.g. as opposed to protein and double-stranded DNA absorbance at 280 and 260 nm respectively). While a full spectrum analysis was not performed in these studies, obtaining the spectral progression over time may be able to provide an optical 'signature' for different types or stages of biofilm.

### *3.2. Observation of significant differences in biofilm optical and morphological properties*

In order to evaluate biofilms formed in different quorum sensing environments, three sets of experiments were performed, with one set consisting of operating all three platforms (containing *E. coli* W3110, and *E. coli* MDAI2 grown with and without AI-2) in parallel for 12, 24, 36, 48, 60, and 72 h. The resulting optical and morphological data were compiled and interpreted with the end of understanding the progression of biofilm growth as well as the dependence on quorum sensing activity.

*3.2.1. Evaluation of biofilm optical density over repeated experiments.* The averages of optical density results from repeated experiments are shown in figure 4, demonstrating the degree of variance.

The optical absorbance of the biofilms is shown to vary with respect to the degree of intercellular communication (figure 4). Wild-type biofilms exhibit an initial period of rapid growth within the first 12 h of flow, while MDAI2 biofilms grown with and without extracellular AI-2 show more gradual increases in optical density. The different types of biofilms exhibit different overall changes in optical density; wild-type biofilms are the most optically dense, while *luxS*-null biofilms are the least optically dense. AI-2 addition appears to restore optical density to MDAI2 biofilms; this is reflected by the compiled data shown in figure 4, where the mean optical density change of MDAI2 biofilms grown with AI-2 is approximately equal to wild-type biofilm optical density

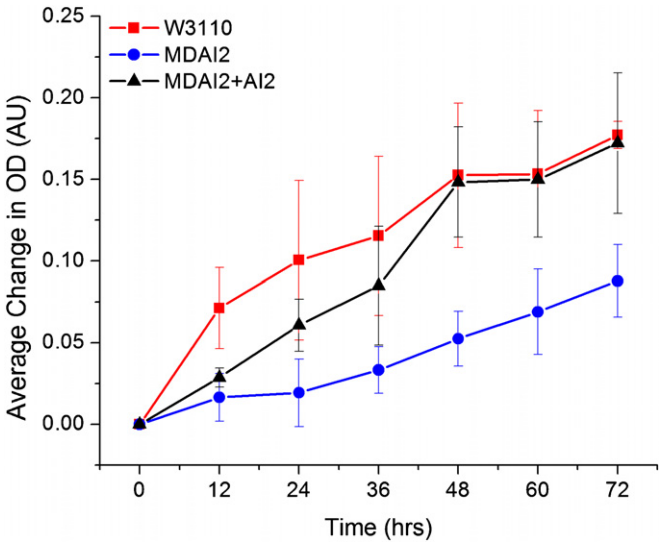


**Figure 4.** Compiled data for the change from baseline optical density for each type of biofilm formed. $n = 3$ for each data point, presented as the average of all trials. Error bars correspond to one standard deviation of the trials.

changes after 48 h. Restoration of the biofilm optical density phenotype by addition of AI-2 confirms the dependence of the biofilm formation on AI-2 within the system. Optical density for all three types of biofilms observed also appears to continue to increase at 72 h and does not appear to approach a steady-state value.

When evaluating the statistical significance of the differences between time points within one strain and between types of biofilms, it was observed that the magnitude of optical changes over growth was not consistent between experiments, reflected in the overlapping error bars in figure 4. However, the relative differences between strains were more consistent between experiments in that wild-type biofilms were consistently the most optically dense, MDAI2 biofilms were the least dense, and by adding AI-2 to the latter, density could be restored. The percent difference between wild-type

**Table 1.** Table of $p$-values obtained through Student's $t$-test for comparison of optical density change magnitude and for comparison of percent difference in optical density change between biofilm groups.

| | 12 h | 24 h | 36 h | 48 h | 60 h | 72 h |
|---|---|---|---|---|---|---|
| W3110 versus MDAI2 | 0.0076 | 0.0129 | 0.0362 | 0.0108 | 0.0224 | 0.0510 |
| W3110 versus MDAI2 + AI2 | 0.0547 | 0.1383 | 0.8478 | 0.8833 | 0.9043 | 0.8713 |
| MDAI2+ AI2 versus MDAI2 | 0.1695 | 0.1247 | 0.0474 | 0.0129 | 0.0264 | 0.0586 |
| % Difference W3110/MDAI2 versus % difference W3110/MDAI2+AI2 | 0.4067 | 0.1755 | 0.0084 | 0.0017 | 0.0146 | 0.0768 |

Differences are considered significant for $p < 0.05$; comparison of strains via percent difference from wild-type biofilms yields more statistically significant differences.

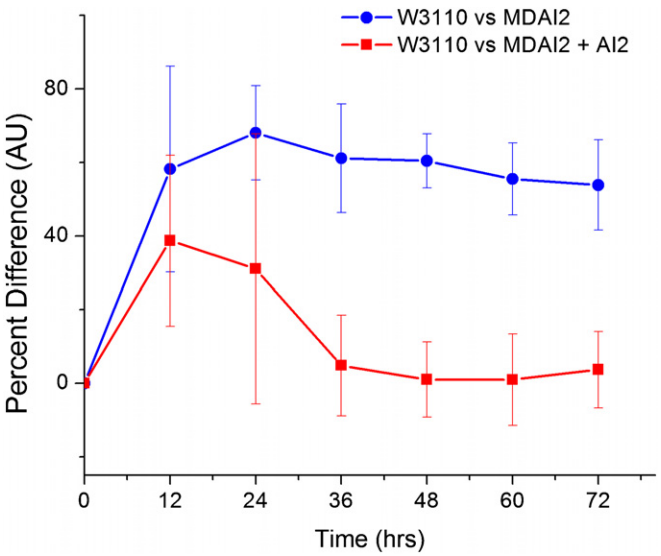


**Figure 5.** Compiled data for the percent difference from wild-type (W3110) biofilms for MDAI2 biofilms (blue circles) and for MDAI2 biofilms grown with AI2 (red squares). Error bars represent one standard deviation of the averaged data.

biofilms and MDAI2 biofilms grown with or without AI-2 is expressed as

$$\%\,\text{Difference} = 100 \times \frac{\text{OD}_w - \text{OD}_x}{\text{OD}_w},$$

using the optical density change of the wild-type biofilm ($\text{OD}_w$) as a reference for the optical density change of MDAI2 grown with or without AI2 ($\text{OD}_x$). Comparison of the percent difference from wild-type biofilms yields more statistically significant differences between biofilm types (figure 5, table 1).

*3.2.2. Evaluation of biofilm morphology over repeated experiments.* Through confocal imaging and analysis of image stacks, the physical nature of the biofilm was interpreted. Representative confocal microscopy images are shown in figure 6. Using the output of COMSTAT, the mean biofilm thickness and roughness coefficient were also averaged between sets, shown in figures 7(*a*) and (*b*) respectively.

Over the windows imaged using confocal microscopy, the variances in thickness differed to a large extent. In some cases where a thick biofilm did not cover the majority of the window, the standard deviation of the thickness could be as much as 100% of the average biofilm thickness. An alternative metric for examining the spatial non-uniformity of the biofilms formed is the roughness coefficient, as defined by Heydorn *et al* and evaluated using COMSTAT [20]. This parameter is a dimensionless number representative of the percent variation in biofilm thickness. As roughness coefficient trends within one channel were variable, as with the optical density, the values for all windows measured for one type of biofilm at one time point were averaged. Results, shown in figure 7(*b*), indicate a large degree of variability between channels and a lack of significant differences between types of biofilms. The results suggest that biofilm roughness has a minimal dependence on bacterial quorum sensing activity, although wild-type *E. coli* biofilms appear to have average roughness values lower than those of the other two types of biofilms

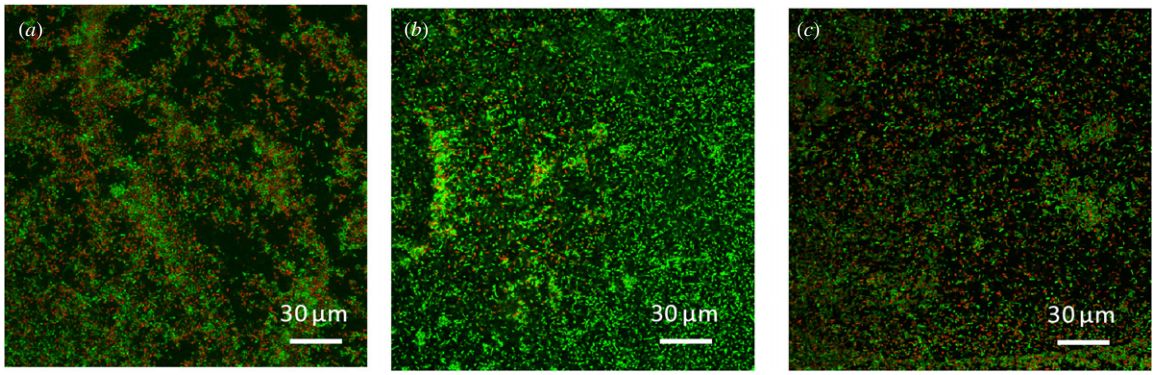


**Figure 6.** Confocal microscopy images of Live/Dead labeled biofilms at 72 h. (*a*) W3110 biofilm, (*b*) MDAI2+AI2 biofilm, (*c*) MDAI2 biofilm. The thickness of each biofilm was 37, 27, and 18 $\mu$m respectively.

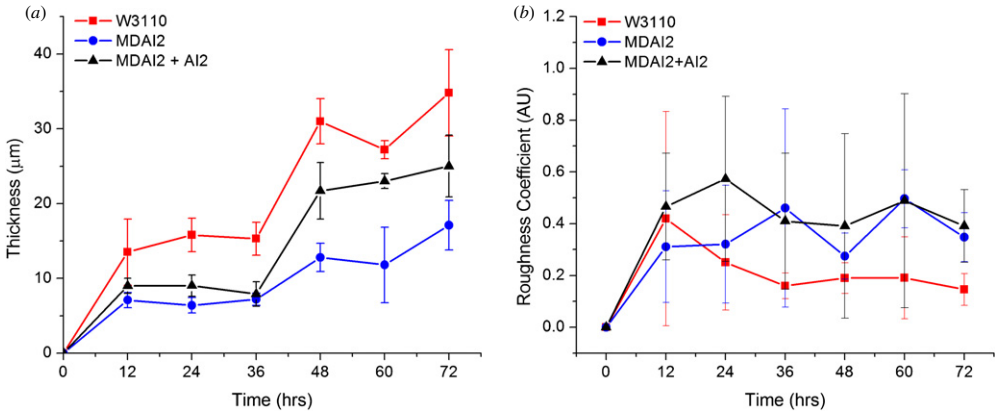


**Figure 7.** Compiled morphological data, including (*a*) average thickness, and (*b*) nondimensional roughness coefficient, for each type of biofilm formed. $n = 3$ for each data point, presented as the average of all trials. Error bars represent one standard deviation of the averaged data.

**Table 2.** Table of *p*-values obtained through Student's *t*-test for comparison of thickness between biofilm groups.

| | 12 h | 24 h | 36 h | 48 h | 60 h | 72 h |
|---|---|---|---|---|---|---|
| W3110 versus MDAI2 | 0.0271 | 0.0004 | 0.0010 | 0.0003 | 0.0008 | 0.0030 |
| W3110 versus MDAI2 + AI2 | 0.0868 | 0.0024 | 0.0015 | 0.0088 | 0.0040 | 0.0380 |
| MDAI2+ AI2 versus MDAI2 | 0.4218 | 0.0973 | 0.6558 | 0.0108 | 0.1456 | 0.0748 |

Differences are considered significant for $p < 0.05$.

investigated, especially after 60 h of growth. Additionally, the variation in the roughness coefficient, indicated by the error bars in figure 7(*b*), is smallest for all three groups at 72 h. This may be indicative of an approach to a steady-state biofilm as the biofilm structure settles to a smooth surface that will not be as prone to sloughing.

The average thickness of the biofilms also shows the same overall trend as the changes in biofilm optical density (figure 7(*a*)). As with the trends in optical density, wild-type biofilms are the thickest, MDAI2 biofilms are the thinnest, and addition of AI-2 to the latter produces MDAI2 biofilms with thickness approaching that of wild-type biofilms. The thicknesses of all the biofilms increase over time, with the most significant increases occurring between 36 and 48 h in W3110 and MDAI2 biofilms grown with AI-2. Thicknesses of biofilms grown in different experiments showed less irreproducibility than the optical measurements and roughness coefficient calculations (figure 7(*a*), table 2).

*3.2.3. Assessment of dependence of biofilm optical density and thickness on growth and quorum sensing.* Both W3110 and MDAI2 form optically detectable biofilms. While MDAI2 is incapable of synthesizing AI-2 due to the lack of *luxS* expression, formation of biofilms, albeit not as efficient as formation of wild-type biofilms, still occurs. This correlates with the work of other groups, who have found that while biofilm formation may be encouraged by quorum sensing, in the absence of quorum sensing bacteria may still form thin, sparse biofilms [21].

Addition of AI-2 appears to restore optical density and thickness to MDAI2 biofilms so that these characteristics approach those of the wild-type biofilms. However, the onset of the restoration is not immediate, as shown in the optical data. It is possible that the concentration of AI-2 used in these studies (30 $\mu$M), combined with the flow properties in microfluidics, may not be sufficient to immediately restore wild-type behavior. While 20 $\mu$M of extracellular AI-2 has produced quorum sensing activity in suspended cultures of MDAI2 [22], the dynamics of the microfluidic reactor may require higher concentrations of AI-2 in the growth media. While the concentration of AI-2 throughout the media is assumed to be uniform at the channel inlet, laminar flow around the biofilm structure and bacterial uptake of AI-2 will produce a non-uniform concentration profile throughout the channel. Conversely to suspensions of MDAI2, the physical structure of the biofilm will also impede transport of AI-2 through the biofilm to bacteria at the substrate interface. Therefore, AI-2 concentrations that may restore quorum sensing activity in a suspended culture of MDAI2 may not produce the same activity in an MDAI2 biofilm formed in a microfluidic flow environment. Additionally, in the regime of microfluidic reactors, the dynamics of AI-2 flow and exposure of the biofilm to AI-2 are expected to vary significantly with dimensions of the microfluidic channel. For future studies using AI-2 or pharmaceutical agents for treating biofilms, the dimensions of the microfluidic reactor must be considered when translating work between studies.

The changes in biofilm optical density from recorded baseline values for all three types of biofilms investigated appear to continue to increase steadily at the end of the selected growth period of 72 h. Conversely, biofilm thicknesses do not appear to exhibit any distinct increase toward the end of the growth period; while longer experiments must be performed in order to confirm or reject the achievement of steady-state thickness in biofilms by 72 h, it may be inferred that the optical density of a biofilm is a unique characteristic, independent

of its thickness. While biofilms may achieve a steady-state thickness, the structure may continue to reorganize itself over time, contributing to increased optical density. The results achieved also correspond with those achieved by Bakke *et al* at the macroscale, in that a morphological steady state was achieved more quickly than an optical steady state [14].

Biofilm thickness does not approach a distinct steady state within the allotted 72 h time period. However, with a longer experimental duration, it is expected that a steady-state thickness would be reached. The attainment of a steady state is expected given the bacterial growth behaviors observed in macroscale settings. When bacteria are grown in any type of reactor, the growth rate is dependent on nutrient availability. In suspension or in static reactors such as a microwell plate, the amount of growth media and nutrients is fixed; therefore, as metabolites are depleted, the bacteria will reach a stationary phase and, given further time, will begin to die [23]. In a flow reactor, there is a continuous supply of fresh nutrients, encouraging continuous and efficient bacterial growth. However, as the biofilm forms on the bottom of the channel, the availability of nutrients to the bacteria at the substratum becomes limited by diffusion through the upper portion of the biofilm, causing the growth rate to slow and eventually approach a steady state as a balance is achieved between thickness and nutrient diffusion. Biofilm thickness is also limited by the shear stress imposed on the biofilm surface, since high amounts of shear will cause bacterial shedding. This limiting effect is particularly pronounced in a microfluidic environment such as that constructed in this work; the small dimensions of the channel (100 $\mu$m deep) imply that as the biofilm grows to thicknesses of tens of microns, the biofilm itself will affect the flow by decreasing the effective diameter of the microfluidic channel and thereby increasing shear stress. Through a negative feedback system, the bacteria will consume nutrients and divide in order to sustain the population but will maintain a thickness small enough for unimpeded flow through the channel (i.e. the channel does not become clogged with biofilm) [4]. The combination of biological and physical phenomena is expected to produce the eventual steady-state thickness suggested by the data in figure 7(*a*).

Of note is the difference in steady-state behavior, or lack thereof, in individual optical density results versus compiled results. As shown in figure 2, individual biofilms exhibit steady-state behavior with an onset within the 72 h testing period, while the compiled optical density results do not appear to reach such a steady state. This is attributed to the different steady-state values of change in optical density that are observed for biofilms formed under the same conditions in different experiments. As with the expected steady-state-biofilm thickness, a longer experimental test period may aid in observing an optically detectable steady-state biofilm in the compiled results, since it is expected that the microfluidic channel itself will limit biofilm growth.

While additional experiments with longer time durations will clarify the dynamics of biofilm formation, it must also be acknowledged that the earlier time points are of more interest than later points in biofilm growth. In terms of the ultimate application of this platform for evaluation of drugs for biofilm prevention and eradication, focusing on early biofilm growth is of particular importance for prevention of serious biofilm infection. Therefore, while it is of scientific interest to continue biofilm growth experiments for longer periods of time, such as the weeks-long experiments performed by Bakke *et al* [14], for the target application of this platform these experiments are not essential.

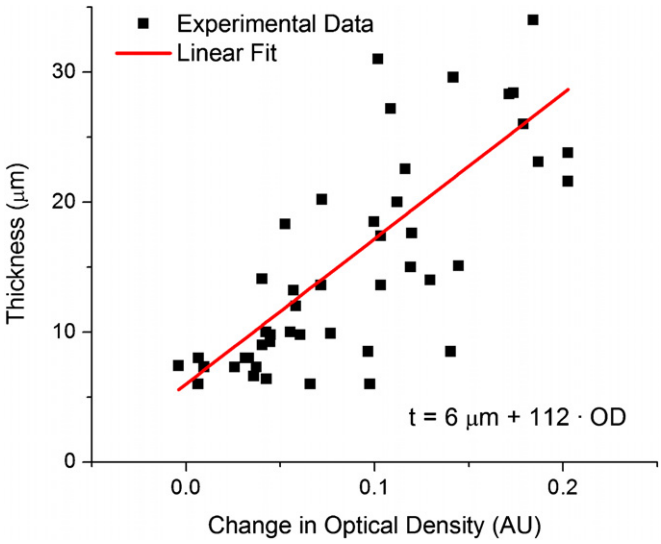


**Figure 8.** Least-squares regression fit of biofilm thickness ($t$) versus change in optical density (OD), compiled for all biofilms at all time points observed. $R^2 = 0.901\,98$.

### *3.3. Evaluation of the relationship between biofilm thickness and optical density*

Although it appears that the relationship between biofilm morphology and optical density is not direct, especially due to possibly differing time scales of steady-state approach, the likelihood of a relationship between the two was statistically investigated. A simple linear correlation between the values for endpoint optical density and biofilm thickness yielded a correlation coefficient of 0.78. Considering the large number of experiments, this degree of correlation is significant and implies a strong association between the two variables. While thickness and optical density are expected to be independent, a linear fit was generated using optical density as an independent variable and biofilm thickness at that time point as a dependent variable. As shown in figure 8, a linear fit of the thickness with respect to change in optical density yields an $r$-squared of 0.9; due to the clustering of data at low optical density and thickness values, an intercept was imposed on the data, allowing for an improved fit. Note that while the fit is improved, it is not directly physically relevant; here, at the onset of the experiment the thickness is predicted to be 6 $\mu$m, which is highly unlikely provided a monolayer of bacterial cells. Further experimentation, especially at shorter time points, is expected to improve this fit.

The uncertainty of the change in optical density measurement is dependent on a number of factors,

including errors introduced by the inherent properties of the measurement equipment, such as the photodiodes (dark current), data acquisition unit (analog input accuracy), and the measurement circuitry (offset introduced by the transimpedance amplifier). As an example, data were used from the endpoint of an immature biofilm with a final optical density change of 0.01; this represents the minimum relevant change in optical density to be measured and is also the point where the most uncertainty will be introduced. From the components of error and using the assumed biofilm, the experimental uncertainty evaluated as outlined in [24] was approximately 0.06% of the overall change in optical density. Note that this uncertainty does not account for natural variations inherent to bacterial systems, and therefore the large variations in the data obtained in this work are most likely due to biological fluctuations. In order to minimize this uncertainty, it would be ideal to perform more repetitions of the experiments to determine the trends in optical density and morphological changes during biofilm formation; this would additionally aid in the refinement of a model of biofilm optical density versus thickness.

Inclusion of other variables in the optical density model, such as substratum coverage and biomass, may produce an improved fit. However, the objective is ultimately to utilize measurement of changes in optical density as a substitute for microscopic measurement of biofilm bulk properties. The refinement of the simplified thickness versus optical density model eliminates the need for corroboration of optical density results using imaging to obtain morphological properties and would be instrumental in development of a completely integrated microfluidic platform for real-time biofilm monitoring.

## 4. Conclusion

We present a microfluidic platform utilizing optical density monitoring to assess biofilm formation in a continuous, non-invasive manner. Due to their ease of implementation and low cost, the platforms were arrayed in parallel allowing for simultaneous operation and performance of multiple experiments. The platform was used to evaluate differences in biofilms formed under varying degrees of quorum sensing activity. Biofilm growth was evaluated via the change in optical density and was compared to the thickness measured via confocal microscopy. Biofilms formed by *E. coli* incapable of quorum sensing molecule synthesis were less optically dense, thinner, and covered less surface area than wild-type biofilms. Addition of quorum sensing molecules partially restores wild-type biofilm characteristics to non-communicating bacteria. While the optical density changes of each biofilm were shown to be quite variable, relative optical differences between different types of biofilms show more reproducibility. A linear fit was used as a preliminary model for relating observed optical density changes to biofilm thickness. With further experimentation, this model will allow for replacement of microscopy with continuous, non-invasive biofilm evaluation via optical density measurement.

In order to fully translate the platform from the current implementation to the final goal of an automated lab-on-a-chip for biofilm monitoring in response to drug treatment, several improvements to the platform itself must be implemented in addition to expansion of the data for the biofilm model. Several microfluidic channels may be fabricated on the same chip, allowing for further compression of the current implementation of one channel per chip. In this vein, an array of photodiodes may be integrated into the substrate, eliminating the need for external optical measurement. In order to simplify the addition of reagents, such as candidate drugs inhibiting quorum sensing, the microfluidic layout should allow for timed introduction and mixing of these reagents into the growth media in order to eliminate variability introduced by changing growth media mid-experiment. The above adjustments will yield a more compact and streamlined device, which will allow for multiple measurements of treated and untreated biofilms in a small, effective, and convenient platform. The platform and methodology presented in this work provide the base for the development of this ideal lab-on-a-chip for evaluation of drugs targeting biofilm formation.

## Acknowledgments

This work was funded by the R W Deutsch Foundation and the National Science Foundation Emerging Frontiers in Research and Innovation (NSF-EFRI) program. The authors appreciate the support of the Maryland NanoCenter and its FabLab. The authors also appreciate the assistance of Amy Beaven with confocal imaging at the University of Maryland Imaging Core Facility. They would additionally like to thank their collaborators in the Maryland Biochip Collaborative and colleagues in the MEMS Sensors and Actuators Laboratory at the University of Maryland.

## References

[1] Potera C 1999 Microbiology—forging a link between biofilms and disease *Science* **283** 1837–9
[2] Stewart P S 2002 Mechanisms of antibiotic resistance in bacterial biofilms *Int. J. Med. Microbiol.* **292** 107–13
[3] Weibel D B, DiLuzio W R and Whitesides G M 2007 Microfabrication meets microbiology *Nat. Rev. Microbiol.* **5** 209–18
[4] Janakiraman V, Englert D, Jayaraman A and Baskaran H 2009 Modeling growth and quorum sensing in biofilms grown in microfluidic chambers *Ann. Biomed. Eng.* **37** 1206–16
[5] Lee J H, Kaplan J B and Lee W Y 2008 Microfluidic devices for studying growth and detachment of *Staphylococcus epidermidis* biofilms *Biomed. Microdevices* **10** 489–98
[6] Kim J, Hegde M and Jayaraman A 2010 Co-culture of epithelial cells and bacteria for investigating host–pathogen interactions *Lab Chip* **10** 43–50
[7] Barrios A F G, Zuo R J, Hashimoto Y, Yang L, Bentley W E and Wood T K 2006 Autoinducer 2 controls biofilm formation in *Escherichia coli* through a novel motility quorum-sensing regulator (mqsr, b3022) *J. Bacteriol.* **188** 305–16
[8] Li J, Attila C, Wang L, Wood T K, Valdes J J and Bentley W E 2007 Quorum sensing in *Escherichia coli* is signaled by ai-2/lsrR: effects on small RNA and biofilm architecture *J. Bacteriol.* **189** 6011–20

[9] Swope K L and Flicklinger M C 1996 The use of confocal scanning laser microscopy and other tools to characterize *Escherichia coli* in a high-cell-density synthetic biofilm *Biotechnol. Bioeng.* **52** 340–56
[10] Prakash S B and Abshire P 2007 On-chip capacitance sensing for cell monitoring applications *IEEE Sens. J.* **7** 440–7
[11] Richter L, Stepper C, Mak A, Reinthaler A, Heer R, Kast M, Bruckl H and Ertl P 2007 Development of a microfluidic biochip for online monitoring of fungal biofilm dynamics *Lab Chip* **7** 1723–31
[12] Yu J, Liu Z, Liu Q, Yuen K T, Mak A F T, Yang M and Leung P 2009 A polyethylene glycol (peg) microfluidic chip with nanostructures for bacteria rapid patterning and detection *Sensors Actuators* A **154** 288
[13] Mannoor M S, Zhang S, Link A J and McAlpine M C 2010 Electrical detection of pathogenic bacteria via immobilized antimicrobial peptides *Proc. Natl Acad. Sci. USA* **107** 19207–12
[14] Bakke R, Kommedal R and Kalvenes S 2001 Quantification of biofilm accumulation by an optical approach *J. Microbiol. Methods* **44** 13–26
[15] Heydorn A, Ersboll B K, Hentzer M, Parsek M R, Givskov M and Molin S 2000 Experimental reproducibility in flow-chamber biofilms *Microbiology* **146** 2409–15
[16] Lowery C A, Dickerson T J and Janda K D 2008 Interspecies and interkingdom communication mediated by bacterial quorum sensing *Chem. Soc. Rev.* **37** 1337–46
[17] Meyer M T, Roy V, Bentley W E and Ghodssi R 2010 A microfluidic device for optical absorbance monitoring of biofilms *IEEE Sensors 2010 (Waikoloa, HI)* pp 2291–4
[18] DeLisa M P, Valdes J J and Bentley W E 2001 Mapping stress-induced changes in autoinducer AI-2 production in chemostat-cultivated *Escherichia coli* K-12 *J. Bacteriol.* **183** 2918–28
[19] Fernandes R and Bentley W E 2009 AI-2 biosynthesis module in a magnetic nanofactory alters bacterial response via localized synthesis and delivery *Biotechnol. Bioeng.* **102** 390–9
[20] Heydorn A, Nielsen A T, Hentzer M, Sternberg C, Givskov M, Ersboll B K and Molin S 2000 Quantification of biofilm structures by the novel computer program COMSTAT *Microbiology* **146** 2395–407
[21] Davies D G, Parsek M R, Pearson J P, Iglewski B H, Costerton J W and Greenberg E P 1998 The involvement of cell-to-cell signals in the development of a bacterial biofilm *Science* **280** 295–8
[22] Roy V, Fernandes R, Tsao C Y and Bentley W E 2010 Cross species quorum quenching using a native AI-2 processing enzyme *ACS Chem. Biol.* **5** 223–32
[23] Zwietering M H, Jongenburger I, Rombouts F M and van't Riet K 1990 Modeling of the bacterial growth curve *Appl. Environ. Microbiol.* **56** 1875–81
[24] Holman J P 1994 *Experimental Methods for Engineers* (New York: McGraw-Hill) pp 49–56